CHAPTER 147

WAVE ENERGY DISSIPATION IN ARBITRARILY SHAPED HARBOURS OF VARIABLE DEPTH

J.K. Kostense*, K.L. Meijer*, M.W. Dingemans*,
A.E. Mynett* and P. van den Bosch*

ABSTRACT

A finite element model for combined refraction-diffraction problems of linear water waves has been extended to include the effect of various dissipative mechanisms on wave excitation response in harbours of arbitrary shape and variable depth. Especially, the effects of bottom friction, partial absorption along the harbour contours, and transmission through permeable breakwaters have been considered. Although, within the mild slope approximation, the model is valid for arbitrary wave lengths, in this paper its effectiveness for harbour design applications is demonstrated for long wave induced resonance phenomena. For this purpose a realistic harbour geometry has been selected. A hydraulic scale-model of this harbour enabled experimental verification of the computational results.

1. INTRODUCTION

The propagation of linear time-harmonic waves in areas of variable depth can be described by the mild-slope equation, as derived by Berkhoff (1972). He solved the equation using a hybrid finite element method, representing the solution in the exterior by a continuous distribution of sources along the radiating boundary. A more elegant approach, resulting in symmetric matrices, was formulated by Chen and Mei (1974). They used a series expansion in terms of Hankel functions for the radiating waves and included the unknown expansion coefficients in a variational formulation.

After the introduction of a partially reflective boundary condition, Berkhoff (1976) could use his model to compute the wave disturbance in harbours with arbitrary reflective properties. As all absorbing conditions for numerical models, this condition cannot maintain the rate of energy dissipation for waves of different angles of incidence. Behrendt (1985) showed how to approximate the perfect boundary condition to higher order.

Booij (1981) suggested a modification of the mild-slope equation to account for the effect of bottom friction by adding a dissipative term. Dingemans (1985) considered the effect of bottom dissipation for shallow water conditions and shows the analogy between the obtained equations and the modified mild-slope equation. Dalrymple et al. (1984) have given several forms of the extra dissipation term for different energy dissipation mechanisms. Liu et al. (1986) showed that the extra term even can

* Delft Hydraulics, the Netherlands

be used to estimate the effects of reflective and transmissive breakwaters in numerical models based on the parabolic approximation of the mild-slope equation. On the other hand, Behrendt (1985) included the effect of bottom friction in the original mild-slope equation by formulating the energy loss as a flux of complex energy through the bottom.

Especially for very long waves the energy loss at the harbour entrance due to flow separation may be important. The modelling of a quadratic flow separation term can be incorporated in a numerical model by amending the matching conditions for pressure and normal velocity at the harbour entrance, see e.g. Berger (1986), who considered diffraction only.

Dissipation mechanisms may have a considerable influence on the wave disturbance in harbours, either for short period wind waves and swell, or for long period waves (tsunamis etc.), or both. For long waves resulting in harbour resonances the peak amplitudes at resonance are influenced by a number of mechanisms, see e.g. Mei (1983):

- radiation damping, i.e. energy escaping seaward from the harbour entrance,
- partial absorption along harbour boundaries due to wave breaking and frictional losses, including internal losses in permeable breakwaters,
- bottom friction,
- flow separation near the harbour entrance,
- finite-amplitude effects of energy transfer into higher harmonics.

Apart from the finite-amplitude effects, all these mechanisms can be accounted for in a newly developed numerical model solving the mild-slope equation. When finite-amplitude effects are expected to be the dominant mechanism, a model based on the Boussinesq equations for shallow water conditions could be applied, see e.g. Abbott et al. (1978).

The newly developed model solves the modified mild-slope equation accounting for bottom friction, and is equipped with a variety of options for appropriate boundary conditions, including one for combined reflection and transmission. To illustrate the effectiveness of the model for harbour design, a series of long wave computations is discussed for one specific realistic harbour geometry (see Fig. 1). Part of these computations have been compared with hydraulic scale-model experiments.

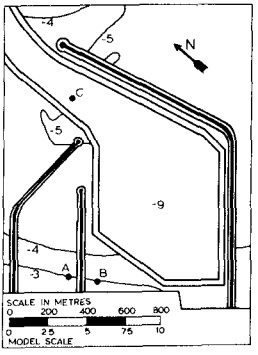

Figure 1 Harbour geometry

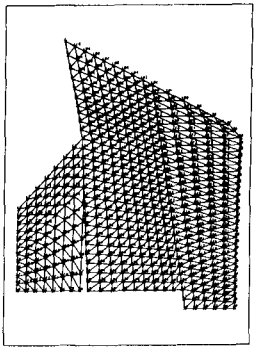

Figure 2 Finite-element grid no. 1

2. MODIFIED MILD SLOPE EQUATION

The mild-slope equation as derived by Berkhoff (1972, 1976) is a two-dimensional depth-integrated elliptic wave equation governing the propagation of linear time-harmonic waves in areas of moderate slope. The modified equation including the dissipation term as suggested by Booij (1981) reads

$$\nabla.(cc_g\nabla\phi) + cc_g(k^2 + ik\gamma)\phi = 0, \tag{1}$$

where $\phi(x,y)$ denotes the two-dimensional velocity potential in the horizontal plane, related to the total potential $\Phi(x,y,z,t)$ according to

$$\Phi(x,y,z,t) = \phi(x,y)\,\frac{\cosh k(h+z)}{\cosh kh}\,e^{-i\omega t}. \tag{2}$$

In Eq. 1, c, c_g and k represent the phase velocity, the group velocity and the wave number, respectively, which can be evaluated from the linear dispersion relation. The funtion γ is defined as W/c_g, where W is the rate of energy dissipation per unit wave energy intensity.

In order to derive Eq. 1, including the effect of energy dissipation due to bottom friction, the principle of virtual work may be employed. Notice in this respect that the original mild-slope equation was obtained by application of a variational principle, and that variational principles are especially suited for conservative systems. However, this approach would be rather intricate and will not be followed here. Instead, Eq. 1 will be made plausible by showing the analogy to the result for shallow water waves. For the case of shallow water, the vertically integrated continuity equation and the horizontal momentum equation read in linearized form

$$\frac{\partial\eta}{\partial t} + \nabla.(\vec{hu}) = 0 \quad , \quad \frac{\partial\vec{u}}{\partial t} + g\nabla\eta + \frac{\vec{\tau}}{\rho h} = 0 \ , \tag{3}$$

where $\vec{\tau}$ is the bottom shear stress vector, for which the friction law

$$\vec{\tau} = \frac{1}{2} f_w \rho |\vec{u}_b| \vec{u}_b \tag{4}$$

is taken, where $\vec{u}_b$ is the wave velocity just outside the bottom boundary layer. With $\vec{u}_b = \vec{u}/\cosh kh$, according to linear theory, the term $\vec{\tau}/\rho h$ is linearized as $W\vec{u}$, so as to obtain the same amount of dissipation over one wave period. This results in

$$W = \frac{4f_w}{3\pi h}\,\frac{1}{(\cosh kh)^2}\,u_e, \tag{5}$$

where f_w is the wave friction coefficient, and u_e represents the effective amplitude of the horizontal velocity

$$u_e = \frac{3\pi}{8}\int_0^T(\vec{u}.\vec{u})^{3/2}dt \;/\; \int_0^T(\vec{u}.\vec{u})dt \ . \tag{6}$$

The product $(\vec{u}.\vec{u})$ can be written as

$$\vec{u}.\vec{u} = p + q\cos(2\omega t - \alpha), \tag{7}$$

where p and q are functions of the derivatives of the real and imaginary parts of the velocity potential $\phi(x,y)$ with respect to x and y. Substituting Eq. 7 into Eq. 6, one obtains after some algebraic manipulation

$$u_e = \sqrt{p+q}\ \{E(m) - \frac{1}{4}(1 - \frac{q}{p})K(m)\}, \qquad m = \frac{2q}{p+q}\ , \tag{8}$$

in which K(m) and E(m) denote the complete elliptic integrals of the first and second kind, respectively, and m is the elliptic parameter. Notice that for p=q the horizontal velocity components are in phase, and the effective velocity amplitude equals the amplitude of the unidirectional velocity $\hat{u}$. Upon combination of the continuity and the momentum equation, and introducing the velocity potential, one obtains for time-harmonic motion

$$\nabla.(gh\nabla\phi) + gh(k^2 + \frac{ikW}{\sqrt{gh}})\phi = 0\ . \tag{9}$$

Because of the close resemblance between this equation and the unmodified mild-slope equation for shallow water, where $c = c_g = \sqrt{gh}$, it seems reasonable to model wave dissipation in the mild-slope equation according to Eq. 1.

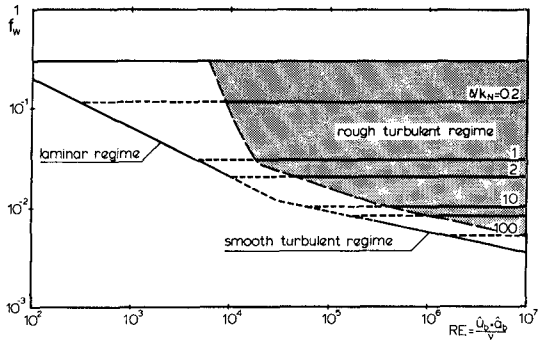

Figure 3 Wave friction coefficient f_w for different boundary layer regimes, see Jonsson (1978)

To determine the wave friction coefficient f_w, as defined in Eq. 4, the relations derived by Jonsson (e.g. 1978) have been used. Jonsson distinguishes three relations for the different types of boundary layers (see Fig. 3):

- laminar regime: $f_{w,l} = 2\ (RE)^{-0.5}$ (10)
- smooth-turbulent regime: $f_{w,s} = 0.09\ (RE)^{-0.2}$ (11)
- rough-turbulent regime: $f_{w,t} = 0.0605/(\log \frac{27\delta}{k_N})^2$. (12)

Moreover, the friction coefficient has a maximum value:

$$f_w \leq 0.30\ . \tag{13}$$

In these relations the amplitude Reynolds number is defined as

$$RE \equiv \frac{\hat{u}_b\ \hat{a}_b}{\nu}\ , \tag{14}$$

where ν denotes the kinematic viscosity, and $\hat{a}_b$ represents the amplitude of the particle excursion at the bed. The thickness of the rough-turbulent boundary layer, δ, can be determined from

$$\delta = 0.072 \ (\hat{a}_b k_N)^{0.25}, \tag{15}$$

where k_N is the well-known Nikuradse roughness parameter. Although the above equations have been derived for unidirectional oscillating flow conditons, $\hat{u}_b$ can be approximated by $u_e/\cosh(kh)$ and $u_e/[\omega\cosh(kh)]$, respectively (see Eq. 6). In nature the boundary layer will always be rough-turbulent. However, as all regimes have been implemented in the numerical model, small-scale hydraulic model conditions can be handled too. This is especially useful for verification studies.

Eq. 1 is solved by means of standard finite element techniques, using triangular elements with linear interpolation functions. The non-linearity, as introduced by the dissipation term, is treated in a straightforward iterative way. If the bottom friction is a predominant dissipation factor, which can be the case for harbour resonance problems, an average number of 3 to 5 iterations appears to be adequate to obtain reliable results. However, if the bottom friction is only a secondary dissipative effect, as for most problems where short wind waves are involved, 2 iterations are already sufficient in most cases.

3. BOUNDARY CONDITIONS

Different types of boundary conditions have been implemented in the finite element model, viz.

- radiation conditions,
- a wave-maker condition,
- a condition for partial reflection, and
- a condition for combined partial reflection and transmission.

Radiation damping can be treated in two ways. Both methods match the finite element region and the outer region, where constant depth is assumed by requiring the continuity of pressure and normal velocity. The first method, applied by Berkhoff (1972, 1976), is to represent the solution in the outer region by a continuous distribution of sources along the open boundary:

$$\phi_s = \int_A u(M) \frac{1}{2i} H_0^1(kr) \, ds \ , \tag{16}$$

where ϕ_s is the velocity potential of the scattered waves, A is the open boundary, and $H_0^1(kr)$ denotes the Hankel function of the first kind and zero'th order. The unknown source strength $\mu(M)$ at point M must be solved along with the inner region by requiring the two matching conditions. Chen and Mei (1974) succeeded to incorparate the matching conditions as natural boundary conditions in a variational principle by representing the velocity potential of the scattered waves as a series expansion of Hankel functions,

$$\phi_s = \sum_{n=0}^{\infty} H_n^1(kr) \ (\alpha_n \cos n\Theta + \beta_n \sin n\Theta) \ , \tag{17}$$

where r and Θ are polar co-ordinates. Again, the coefficients α_n and β_n are determined by matching with the solution in the inner region. Both methods have been implemented in the numerical model. In general, the second method is to be recommended, as it results in a symmetric matrix. However, as the region to be modelled will generally be larger for this method, sometimes the source method may be preferable, especially for harbours and bays with wide openings.

To be able to compare with hydraulic model experiments, a wave-maker condition is very useful. The implemented condition reads

$$\frac{\partial \phi}{\partial n} + ik\tilde{\phi} = 0 \ , \tag{18}$$

where $\tilde{\phi}$ is the velocity potential of the generated waves, and n is the direction normal to the wave paddle. As can be simply derived, Eq. 18 implies a 100% reflective paddle.

Partially reflective harbour contours are modelled with the well-known equation (see e.g. Berkhoff, 1976)

$$\frac{\partial \phi}{\partial n} - ik(1-r)\phi = 0 \ . \tag{19}$$

This condition will work for all kinds of incident wave systems in regions of variable depth, and for curved boundaries. However, to relate the actual reflection coefficient R to the complex coefficient r, a long-crested wave incident on a straight boundary in constant water depth is assumed, i.e.

$$\phi = \phi_i e^{i(kx\cos\alpha - ky\sin\alpha)} + R\phi_i e^{i(kx\cos\alpha + ky\sin\alpha + \rho)} , \tag{20}$$

where ρ denotes the phase shift at the boundary. Subsitution in Eq. 19 yields

$$Re^{i\rho} = \frac{\sin\alpha - 1 + r}{\sin\alpha + 1 - r} , \tag{21}$$

showing the dependence of R on the angle of incidence α.

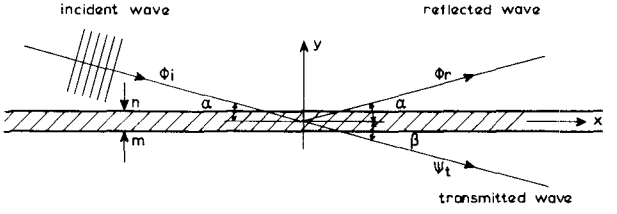

Figure 4 Definition sketch for a transmitting boundary

Analogously to Eq. 19 a boundary condition for combined reflection and transmission has been developed, assuming equal reflection and transmission characteristics in both directions, i.e. symmetrical constructions. The velocity potentials on either side of the transmitting boundary are denoted as ϕ and ψ, where

$$\phi = \phi_o + \phi_t \quad , \quad \psi = \psi_o + \psi_t . \tag{22,23}$$

The subscript t refers to that part of the local potential which originates from transmission, see Fig. 4 for a reference sketch. The general form of the boundary condition consists of the following set of four equations

$$\psi_t = s\phi_o \quad , \qquad \phi_t = s\psi_o \tag{24,25}$$

$$\frac{\partial\phi_t}{\partial m} = -t\frac{\partial\phi_o}{\partial n} \quad , \qquad \frac{\partial\phi_t}{\partial n} = -t\frac{\partial\psi_o}{\partial m} \quad , \tag{26,27}$$

where s and t are complex coefficients. Eq. 19 for ϕ_o and a similar one for ψ_o, Eqs. 22, 23 and similar ones for the normal derivatives of the potential, and Eqs. 24 to 27 constitute a set of 10 equations for 12 unknowns. Elimination yields the following two equations in terms of the potentials ϕ and ψ, and their respective normal derivatives:

$$(1-s^2)\frac{\partial\phi}{\partial n} - ik(1-r)\{(1+st)\phi - (s+t)\psi\} = 0 \tag{28}$$

$$(1-s^2)\frac{\partial\psi}{\partial m} - ik(1-r)\{(1+st)\psi - (s+t)\phi\} = 0 \ . \tag{29}$$

Across the boundary the velocity potential jumps discontinuously, which can be numerically treated by means of line elements with double nodes. To achieve full reflection for r = 1, as well as non-transmission for t = 0, the coefficient s has been taken to be

$$s = (1-r)t \ . \tag{30}$$

Again assuming long-crested waves in constant water depth, the velocity potential on either side of the boundary may be described by Eq. 20 along with

$$\psi = T\phi_I e^{i(kx\cos\beta - ky\sin\beta + \tau)} , \tag{31}$$

where τ denotes the phase shift of the transmitted wave over the barrier, see also Fig. 4 for the reference system. For $\beta = \alpha$, substitution of Eqs. 20 and 31 in Eqs. 28 to 30 yields

$$Re^{i\rho} = \frac{-t^2(1-r)^2(1-\sin\alpha)(1+\sin\alpha) + (1-r+\sin\alpha)(1-r-\sin\alpha)}{+t^2(1-r)^2(1-\sin\alpha)^2 - (1-r+\sin\alpha)^2} \quad \text{and} \tag{32}$$

$$Te^{i\tau} = \frac{-2t(1-r)(2-r)\sin\alpha}{+t^2(1-r)^2(1-\sin\alpha)^2 - (1-r+\sin\alpha)^2} \ . \tag{33}$$

As an example, for t = 1 and $\rho = \tau = 0$ these equations result in

$$R + T = 1 \ , \tag{34}$$

which implies a rate of energy dissipation

$$D = 1 - R^2 - T^2 . \tag{35}$$

Eq. 34 has been derived by Madsen and White (1975) for a permeable breakwater and long waves. Fig. 5 shows the dependency of R and T on the angle of incidence, also for t = 1 and $\rho = \tau = 0$. For normally incident waves Eqs. 32 and 33 reduce to

$$Re^{i\rho} = \frac{r}{2-r} \qquad \text{and} \qquad Te^{i\tau} = \frac{2t(1-r)}{2-r} \ . \tag{36,37}$$

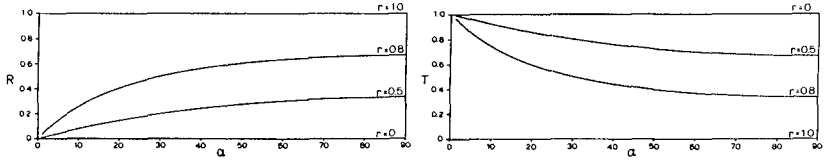

Figure 5 Reflection (R) and transmission (T) coefficients as functions of the angle of incidence (α); $t = 1$, $\rho = \tau \approx 0$

Apart from transmission through permeable breakwaters, the transmission conditions might be also applied to approximate the effect of energy loss due to flow separation at the harbour entrance, and at protruding structures within the harbour. The usual formulation for the energy loss at the harbour entrance is

$$\eta^- - \eta^+ = \frac{f_e}{2g} u|u|, \tag{38}$$

where η^- and η^+ denote the free-surface displacements on either side of the constriction, and u is the velocity component normal to the entrance. In the equation the apparent inertia term has been neglected, which is acceptable for long waves. Unfortunately, direct empirical knowledge of the friction coefficient f_e is hardly available, but generally f_e is assumed to be ≤ 1.5.

4. SOME APPLICATIONS FOR A COMPLEX HARBOUR GEOMETRY

The model has been satisfactorily verified for a variety of simple configurations, permitting a comparison with analytical solutions. The verification programme included the classical Homma island surrounded by a parabolic shoal, a rectangular harbour with constant depth, and obliquely incident waves over a linearly sloping bottom with constant depth at both sides. After these verifications the model has been used in normal laboratory advice practice, mostly to study harbour responses due to wind waves and swell. The model has recently been implemented on a CRAY-XMP supercomputer. Taking full advantage of the vector-processor, the sytem of equations is solved quite efficiently. Until now, the largest system which has been solved, referred to a grid of 37,000 nodal points for a 10 second wave computation without bottom dissipation in an area of about 10 km^2. The CPU time to execute this computation was about 2 minutes.

Hereafter, some results of further research will be shown to illustrate the effectiveness of the numerical model to solve harbour resonance problems. It is well known that harbour oscillations induced by long waves may result in considerable hazards for e.g. moored ships. Although a variety of forcings can be responsible for these oscillations, the most studied forcing is due to incident free long waves (tsumamis etc.). Until now, most numerical models mainly predict the natural frequencies of the harbour and the corresponding oscillation modes. However, there is an increasing need for realistic peak amplitudes at resonance, especially for numerical methods to determine the dynamic behaviour of moored vessels inside a harbour, see e.g. Mynett et al. (1985). To examine whether this model could fulfil this need, a series of computations was

performed for a realistic harbour geometry (see Fig. 1). The choice of this specific lay-out enables the comparison with experiments in a physical model having a length scale of 1:80. The harbour area of about 1 km^2 is divided into two parts by an inner breakwater. The main part has been dredged to -9.0 m; the shallow part accomodates fishing-boats etc. All computations and experiments have been carried out for a water level of Chart Datum + 1.25 m. For the computations three different finite element grids have been used, viz.

- grid no. 1, including the harbour area only, and having scale-model dimensions (see Fig. 2),
- grid no. 2, reproducing the scale-model (see Fig. 9), and
- grid no. 3, reproducing the harbour and surroundings at natural scale (see Fig. 13).

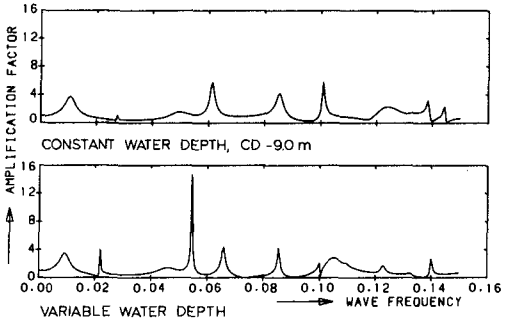

Figure 6 Harbour response at position B for constant and variable depth; radiation damping only, grid no.1

Grid no. 1 was used for some first computations on the effects of the variable depth and the (laminar) bottom friction. The direction of the incident waves was 30° from North (see Fig. 1) and the harbour contours were 100% reflective. Fig. 6 shows for position B (see Fig. 1), that, even for a harbour with constant water depth in its main part, a combined refraction-diffraction model is essential to predict natural frequencies. For the same position, Fig. 7 illustrates the effect of bottom friction, using a Nikuradse roughness of k_N = 0.5 mm, which represents the cemented bottom of a scale model. Even for a very moderate height of the incident waves, H = 1.5 mm, the reduction due to bottom friction can be quite considerable, especially for sharp resonance peaks. For example, the peak at 0.055 Hz, representing a mode with half a wave length between the inner breakwater and the eastern one, is reduced to less than 20% at point B.

A sketch of the lay-out of the physical model is shown in Fig. 8. The long wave experiments have been performed for one wave direction, for which situation the position of the wave generator and two guiding walls have been indicated. Monochromatic waves with a wave height of 3 mm were generated for a series of wave periods between 10 and 40 seconds, excluding the occurrence of wave breaking. Ten wave height gauges were used, including one in the harbour mouth. The measured signals have been Fourier analysed to obtain the wave amplitude in the fundamental frequency. All breakwaters had a 1:2 slope of rough stones and were fully

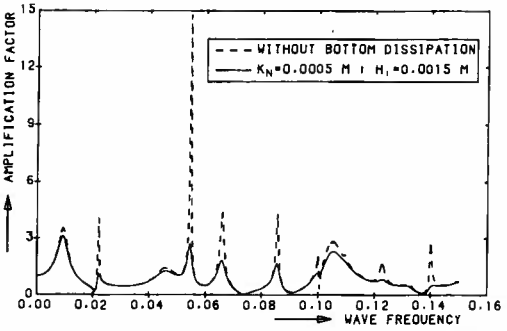

Figure 7 The effect of frictional damping on the harbour response at position B, grid no. 1

impermeable. The boundaries at the south end of the harbour were vertical quays. The finite element grid for the verification study is shown in Fig. 9. The main reason to reproduce the area around the access channel was to be certain of correct wave directions at the harbour mouth. As Fig. 9 shows, the regions behind the guiding walls have not been reproduced. The boundaries at the end of the guiding walls have been supposed to be fully absorbing; all other boundaries were 100% reflective. Earlier computations had revealed that only a marginal absorption rate in the order of 5% can reduce the harbour response at resonance by more than 25%, see also Behrendt (1985). However, such small reductions are hardly measurable in a complex harbour model. Another main reason to expect lower responses in the scale model beforehand, is that the wave generators are not fully reflective, which was assumed in the numerical model, see Eq. 18.

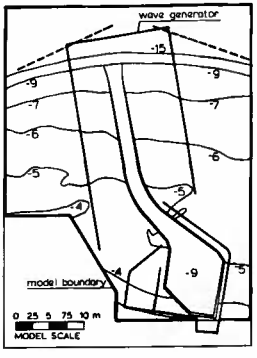

Figure 8 Lay-out of 1:80 scale model

Figure 9 Finite-element grid no. 2

Fig. 10 shows representative examples of the comparison between measurements and computations for two stations. Position A refers to a corner in the shallow basin and position C is situated in the harbour entrance, see Fig. 1. The lowest graph shows the amplification between both stations. Looking at the upper graphs, it is obvious that in general the

computed responses indeed exceed the measured ones. However, especially for two frequencies considerable discrepancies occur, i.e. for f=0.039 Hz and f=0.066 Hz. As shown in Figs. 11 and 12, these specific frequencies induce resonance in the outer area, between the wave generator and the breakwaters. This distance equals one wave length for f = 0.039 Hz and 2.5 wave lengths for f = 0.066 Hz. The discrepancies at these frequencies may be explained by the fact that the wave generator did not reflect the incident wave energy completely, as was assumed in the numerical model. Nevertheless, this hardly explains the large amplification between stations A and C for 0.066 Hz (see Fig. 10). A more thorough examination of this frequency revealed that the amplification was very sensitive for the position of the antinodal line at the harbour entrance. A minor change of this position, due to a slightly different grid in the sharp corner between the western breakwater and the outer boundary, reduced the amplification between stations A and C considerably. Apart from the discussed frequencies, the agreement between measurements and computations is quite satisfactory, especially when considering the amplification between the harbour entrance and positions within the harbour. In general, the computations result in higher responses at resonance frequencies. This may be attributed to the following reasons: minor absorptions along the boundaries, the energy loss due to flow separation at the breakwater ends, and finite-amplitude effects resulting in energy transfer to higher harmonics. The small shifts in the peak frequencies are ascribed to non-linear effects.

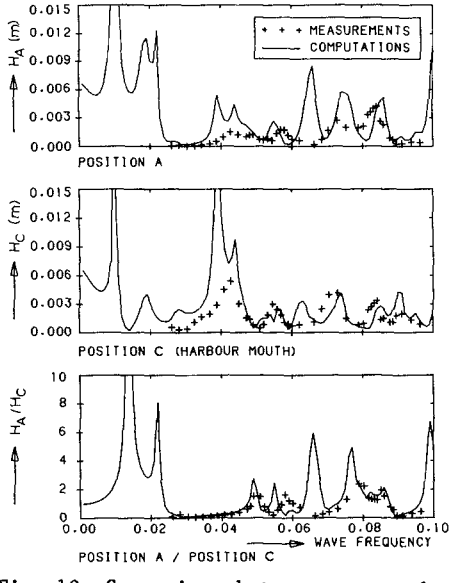

Fig. 10 Comparison between measured and computed harbour response at positions A and C; H_I = 0.003 m, k_N = 0.0005 m

The third set of computations refers to prototype scale, implying turbulent boundary layers. The bathymetry in the grid area is shown in Fig. 13. A constant value of the Nikuradse roughness, k_N = 0.04 m, has been taken for the entire area. Although less dominant than for the laminar case the effect of bottom friction can still be considerable; results will be reported elsewhere. The effects of partial reflection and transmission have been studied for monochromatic waves incident from a direction perpendicular to the main breakwater (70 °), with an incident wave height H = 0.25 m and wave frequencies up to 0.01 Hz. The boundary conditions 28 and 29 have been used for all three breakwaters, whereas the southern boundaries of the harbour have been assumed to be fully reflective for all computations. As an example of the results, the harbour response at position A is compared in Fig. 14 for the following three breakwater characteristics:

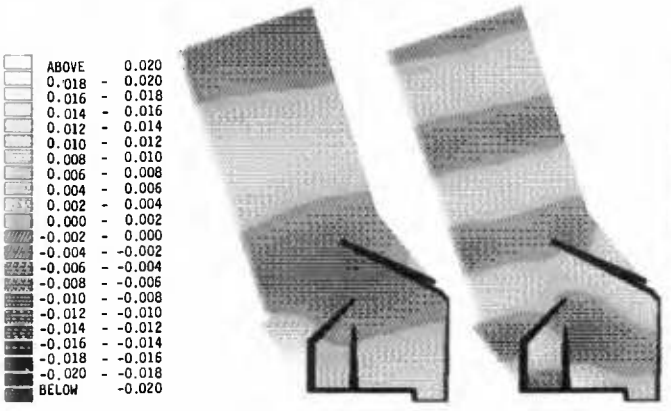

Fig. 11 Free surface contours at the moment of maximum elevation for $f = 0.039$ Hz; $H_I = 0.003$ m, $k_N = 0.0005$ m

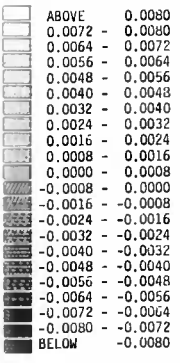

Fig. 12 Free surface contours at the moment of maximum elevation for $f = 0.066$ Hz; $H_I = 0.003$ m; $k_N = 0.0005$ m

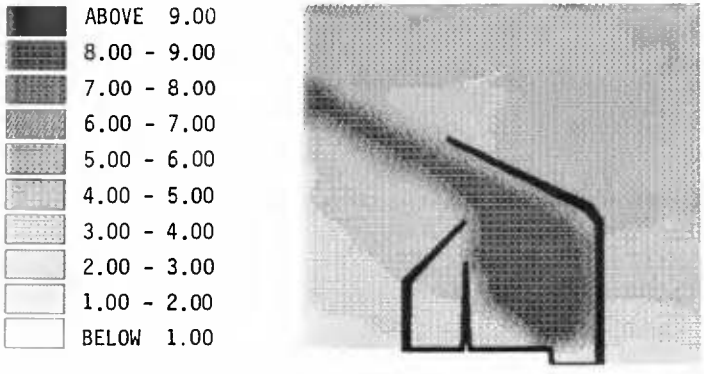

Figure 13 Bathymetry in computational area (grid no.3)

a) full reflection: R = 1.0, T = 0.0
b) partial reflection: R = 0.9, T = 0.0 and
c) partial reflection and transmission: R = 0.9, T = 0.1.

The constants in Eqs. 28 and 29 have been determined from the relations 36 and 37 under condition of no phase shift, i.e. $\rho = \tau = 0$.

A comparison of conditions a) and b), see Fig. 14, shows that a small reduction of R results in a considerable reduction of the amplifications at resonance. The maximum amplification is seen to be about 2, which also holds for other positions within this specific harbour. Although, for impermeable breakwaters a reflection coefficient of R = 1.0 is quite

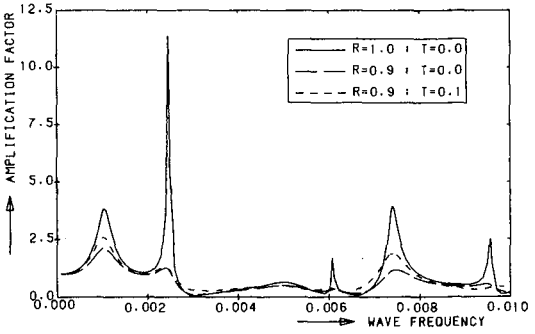

Figure 14 The effect of partial reflection and transmission on the harbour response at position A, grid no. 3

realistic for relatively long waves, condition c) is more appropriate for permeable breakwaters of the rubble mound type, for which T = 0.1 is even a rather low value. As Eq. 35 shows, conditions b) and c) result in almost the same energy loss at the boundaries. However, due to transmission there is an extra inflow of energy through the breakwaters, here primarily through the main breakwater. A comparison of conditions b) and c) in Fig. 14 shows a small increase in amplification due to transmission for all frequencies. It is noted that for other positions the amplifications of c) can also be less than those of b) for parts of the frequency range. The above results suggest that for permeable breakwaters the energy dissipation within the breakwater is of paramount influence on the response characteristics, whille the extra inflow of energy is much less important.

In Fig. 14 the response peak at 0.0246 Hz refers to the Helmholtz mode of the inner shallow basin. The small peak at 0.00608 Hz represents an oscillation mode of the main basin. This mode is shown in Fig 15 for four different conditions, and illustrates again that partially absorbing boundaries may have an enormous effect on peak responses.

5. CONCLUSIONS

A finite element model solving the modified mild-slope equation for waves with arbitrary wave length has been applied to study dissipative effects on harbour resonance phenomena. The effects of bottom friction, partially absorbing boundaries, and also transmission have been considered. To model the effect of combined reflection and transmission, a new boundary condition has been proposed. The following conclusions have been obtained:

- In harbour design studies, it is essential to include the effect of variable depth in the mathematical model to obtain a good prediction of the resonance frequencies.
- Bottom dissipation may be of considerable influence on the harbour response at resonance, both for laminar and turbulent flow regimes.
- Usually, harbour response studies are performed for fully reflective harbour contours. It has been shown that a small reduction of reflection coefficients may result in a drastic decrease of the harbour response at resonance. Such reductions occur in case of permeable rubble mound breakwaters. The effect of the additional inflow of wave

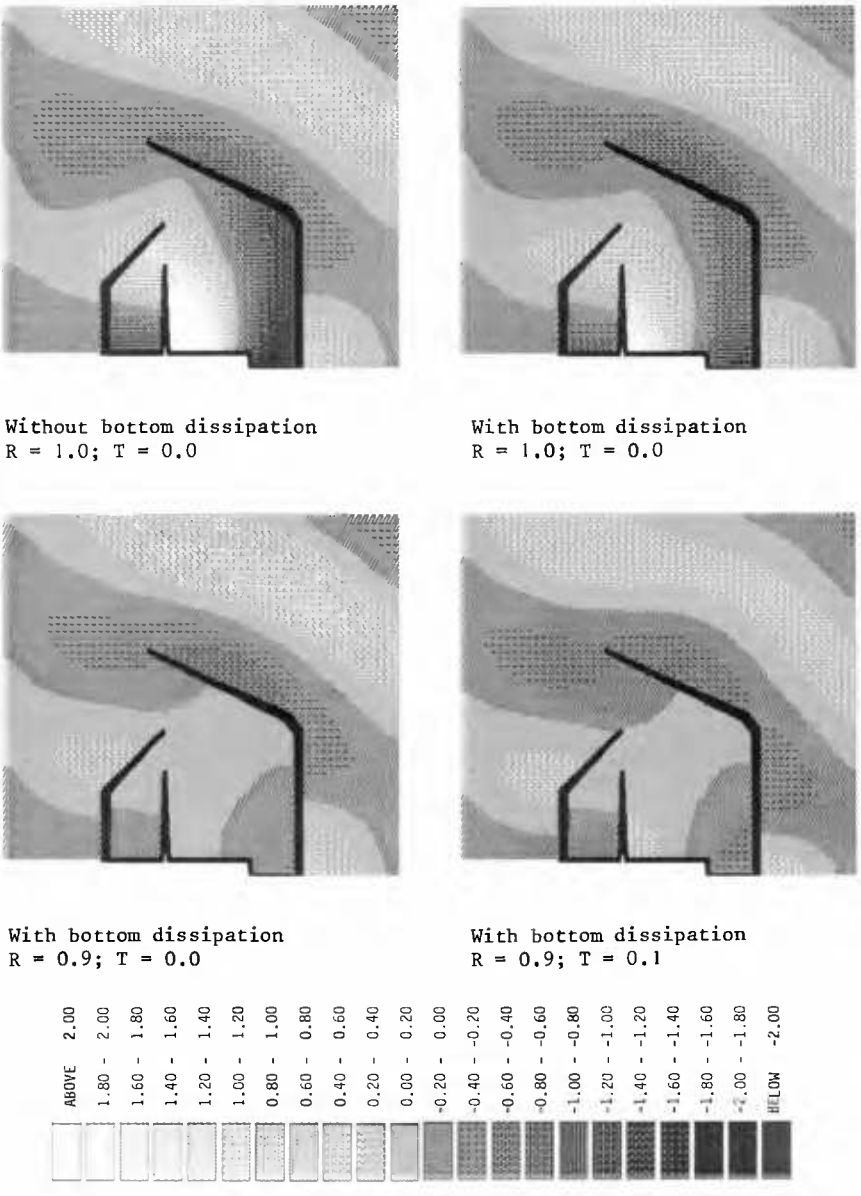

Figure 15 Free surface contours at the moment of maximum elevation for f = 0.00608 Hz; H_I = 0.25 m, k_N = 0.04 m

energy through these breakwaters is found to be less important than the effect of energy dissipation within the breakwater.

- Comparison between measurements in a hydraulic scale model and numerical computations shows a satisfactory agreement in harbour responses. This confirms that, also for long waves, the numerical model is an useful tool for engineering design purposes. The agreement might be even further improved by inclusion of the effect of flow separation in the model. However, for applications it is most essential to represent the appropriate boundary conditions correctly.

REFERENCES

Abbott, M.B., Petersen, H.M. and Skovgaard, O., 1978: On the numerical modelling of short waves in shallow water; J. Hydr. Res., Vol. 16, No. 3, pp. 173-204.

Behrendt, L., 1985: A finite element model for water wave diffraction including boundary absorption and bottom friction; Inst. Hydrodyn. and Hydraulic Engng., Techn. Univ. Denmark, Series Paper no. 37.

Berkhoff. J.C.W., 1972: Computation of combined refraction-diffraction; Proc. 13th Int. Conf. Coastal Engng., ASCE, Vancouver, Vol. 1, Chap. 24, pp. 471-490.

Berkhoff, J.C.W., 1976: Mathematical models for simple harmonic linear water waves, wave diffraction and refraction; Delft Hydraulics Lab., Publ. no. 163.

Booij, N., 1981: Gravity waves on water with non-uniform depth and current; Communications on Hydraulics, Dept. of Civil Engng., Delft Univ. of Techn., Rep. no. 81-1.

Chen, H.S. and Mei, C.C., 1974: Oscillations and wave forces in an offshore harbor; Parsons Lab., Massachusetts Inst. of Techn., Rep. no. 190.

Dalrymple, R.A., Kirby, J.T. and Hwang, P.A., 1984: Wave diffraction due to areas of energy dissipation; J. of Waterway, Port, Coastal and Ocean Engng., ASCE, Vol. 110, No. 1, pp. 67-79.

Dingemans, M.W., 1985: Surface wave propagation over an uneven bottom, evaluation of two-dimensional horizontal wave propagation models; Delft Hydraulics Lab., Rep. no. W310, part 5.

Gerber, M., 1986: Modelling dissipation in harbour resonance; Coastal Engineering, Vol. 10, pp. 211-252.

Jonsson, I.G., 1978: A new approach to oscillatory rough turbulent boundary layers; Inst. Hydrodyn. and Hydraulic Engng., Techn. Univ. Denmark, Series Paper no. 17.

Liu, P.L.-F., Yoon, S.B. and Dalrymple, R.A., 1986: Wave reflection from energy dissipation region; J. of Waterway, Port, Coastal and Ocean Engng., ASCE, Vol. 112, No. 6, pp. 632-644.

Madsen, O.S., and White, S.M., 1975: Reflection and transmission characteristics of porous rubble mound breakwaters; Parsons Lab., Massachusetts Inst. of Techn., Rep. no. 207.

Mei, C.C., 1983: The applied dynamics of ocean surface waves; John Wiley and Sons, New York.

Mynett, A.E., Keuning, P.J. and Vis, F.C., 1985: The dynamic behaviour of moored vessels inside a harbour configuration; Proc. Int. Conf. Numerical and Hydraulic Modelling of Ports and Harbours, IAHR, Birmingham, pp. 211-220.

Skovgaard, O., Behrendt, L. and Jonsson, I.G., 1984: A finite element model for wind wave diffraction, Proc. 19th Int. Conf. Coastal Engng., ASCE, Houston, Vol. 1, Chap. 74, pp. 1090-1102.